Cavity QED in the Ultrastrong Coupling Regime: Photon Bunching from the Emission of Individual Dressed Qubits

Journal:	*ACS Photonics*
Manuscript ID	ph-2017-006355.R1
Manuscript Type:	Article
Date Submitted by the Author:	13-Aug-2017

Complete List of Authors:	Garziano, Luigi; University of Southampton Faculty of Physical Sciences and Engineering, Ridolfo, Alessandro; Universita degli Studi di Messina, Dipartimento di Scienze Matematiche e Informatiche, Scienze Fisiche e Scienze della Terra (MIFT) De Liberato, Simone; University of Southampton, Quantum Light and Matter Group Savasta, Salvatore; Universita degli Studi di Messina, Universita degli Studi di Messina, Dipartimento di Scienze Matematiche e Informatiche, Scienze Fisiche e Scienze della Terra (MIFT)

Cavity QED in the Ultrastrong Coupling Regime: Photon Bunching from the Emission of Individual Dressed Qubits

Luigi Garziano, [†] Alessandro Ridolfo, [‡,¶] Simone De Liberato, [*,†] and Salvatore Savasta [‡,¶]

†*School of Physics and Astronomy, University of Southampton, Southampton, SO17 1BJ, United Kingdom*

‡*Dipartimento di Scienze Matematiche e Informatiche, Scienze Fisiche e Scienze della Terra (MIFT), Università di Messina, I-98166 Messina, Italy*

¶*CEMS, RIKEN, Saitama 351-0198, Japan*

E-mail: S.De-Liberato@soton.ac.uk

Abstract

Photon antibunching in the light scattered by single quantum emitters is one of the hallmarks of quantum optics, providing an unequivocal demonstration of the quantized nature of the electromagnetic field. Antibunching can be intuitively understood by the need for a two-level system lying in its lower state after emitting a photon to be re-excited into the upper one before a second emission can take place. Here we show that such a picture breaks down in the ultrastrong light-matter coupling regime, when the coupling strength becomes comparable to the bare emitter frequency. Specializing to the cases of both a natural and an artificial atom, we thus show that a single emitter

coupled to a photonic resonator can emit bunched light. The result presented herein is a clear evidence of how the ultrastrong coupling regime is able to change the nature of individual atoms.

Keywords

Cavity QED, Two-photon correlation function, Ultrastrong coupling.

1 Introduction

The nonclassical phenomenon of photon antibunching [1] was first observed in the resonance fluorescence of sodium atoms in a low-density atomic beam. [2] Since then, this phenomenon has been observed in a variety of single quantum emitters as trapped ions, dye molecules, [3] semiconductor quantum dots, [4–6] nitrogen-vacancy centers in diamond, [7,8] single carbon nanotubes, [9] and superconducting qubits. [10] Apart from its fundamental importance, it can be used for the realization of triggered single-photon sources, [11] an important building block of quantum technology architectures. [12–14] The efficiency of triggered single photon sources can be significantly improved by coupling the quantum emitter to a single mode of an electromagnetic cavity with dimensions comparable to the emission wavelength. [5,15,16] If the interaction rate λ between the atomic dipole and the electromagnetic field amounts to a non negligible fraction of the atomic transition frequency ω_a, the routinely invoked rotating-wave approximation (RWA) is no longer applicable and the antiresonant terms in the interaction Hamiltonian significantly change the standard cavity QED scenarios. [17–37] In particular, it has been shown that this regime can significantly modify the statistics of cavity photons. [38–40] This light-matter ultrastrong coupling (USC) regime has been experimentally reached in a variety of solid state systems. [41–50] Specifically, superconducting circuits have proven to be the most exquisite platform for microwave on-chip quantum-optics experiments in the USC regime. [42,43,51,52] First- and second-order correlation function measurements have been per-

formed in these systems by using quadrature amplitude detectors and linear amplifiers.[53–55] Moreover, the deep strong coupling regime, where the coupling strength becomes comparable or even larger than the atomic and cavity frequencies, has been recently achieved in a superconducting flux qubit tunably coupled to an LC oscillator via Josephson junctions.[50]

Here we study the statistics of photons emitted by a two-level system ultrastrongly coupled to a photonic resonator (see Fig. 1), rising the question if the antibunching of photons emitted by a single atomic-like transition is a general feature of individual quantum emitters, or, on the contrary, there are cases where photon bunching can be observed. Crucially, while the two-photon correlation function of light transmitted through an optical cavity can display a great variety of behaviours depending on the cavity-embedded quantum system,[56] the zero-delay photon-photon correlation function for light emitted by a single two-level system is known to be zero by definition. Surprisingly, our results will show how, accordingly to the specificity of the system and to the strength of the light-matter coupling, situations arise where the standard antibunching effect does not occur and the two-level system emits light displaying a zero-delay two-photon correlation function significantly different from zero.

The quantum operator describing the electric field can be written as[57,58]

$$\hat{\mathbf{E}}(\mathbf{r},t) = \hat{\mathbf{E}}_{\rm in}(\mathbf{r},t) - \mathbf{\Psi}(\mathbf{r})\,\ddot{\hat{\sigma}}_x(\tilde{t})\,, \tag{1}$$

where $\hat{\mathbf{E}}_{\rm in}(\mathbf{r},t)$ is the incoming field, $\hat{\sigma}_x = \hat{\sigma}_+ + \hat{\sigma}_-$ with $\hat{\sigma}_\pm$ the atomic rising and lowering operators, $\tilde{t} = t - r/c$ with c the speed of light, and $\mathbf{\Psi}(\mathbf{r}) = [\mathbf{d} - (\mathbf{d}\cdot\mathbf{r})\mathbf{r}/r^2]/(c^2 r)$ describes the electric field emitted in the far field region by a point dipole with moment $\mathbf{d}$. Here, $\mathbf{d}\,\hat{\sigma}_x$ is the atomic dipole operator. We notice that the amplitude of the emitted-field operator is proportional to $d\,\ddot{\hat{\sigma}}_x(\tilde{t})$, which is the quantum operator corresponding to the classical amplitude $q\,\dot{v}$, where q and v represent the dipole charge and the relative velocity between the opposite charges of the dipole. According to the quantum theory of photodetection,[59] the probability rate for a photon polarized in the j direction to be absorbed by an ideal

photodetector at point $\mathbf{r}$ at time t is proportional to the normal-order correlation function $\langle \hat{E}_j^-(\mathbf{r},t)\hat{E}_j^+(\mathbf{r},t)\rangle$, where $\hat{E}_j^+$ and $\hat{E}_j^- = (\hat{E}_j^+)^\dagger$ are the jth Cartesian components of the positive- and negative-frequency electric-field operators. This result can be generalized to coincidence probabilities. For example, the probability to detect a photon at point $\mathbf{r}_1$ at time t_1 and a photon at point $\mathbf{r}_2$ at time t_2 is proportional to the normal-order photon-photon correlation function $G^{(2)}(\mathbf{r}_1,t_1;\mathbf{r}_2,t_2) = \langle \hat{E}_j^-(\mathbf{r}_1,t_1)\hat{E}_j^-(\mathbf{r}_2,t_2)\hat{E}_j^+(\mathbf{r}_2,t_2)\hat{E}_j^+(\mathbf{r}_1,t_1)\rangle$.

When the atom evolves freely at its unperturbed frequency ω_a, we have

$$\hat{\sigma}_-(t) = \hat{\sigma}_-(0)e^{-i\omega_a t}, \tag{2}$$

and from Eq. (1) the positive-frequency field takes the form

$$\hat{\mathbf{E}}^+(\mathbf{r},t) = \hat{\mathbf{E}}^+_{\rm in}(\mathbf{r},t) + \mathbf{\Psi}(\mathbf{r})\,\omega_a^2\,\hat{\sigma}_-(\tilde{t}). \tag{3}$$

According to Eq. (3), the normal-ordered, zero-delay second-order correlation function $G^{(2)}(\mathbf{r},t;\mathbf{r},t) = \langle \hat{E}_j^-(\mathbf{r},t)\hat{E}_j^-(\mathbf{r},t)\hat{E}_j^+(\mathbf{r},t)\hat{E}_j^+(\mathbf{r},t)\rangle$, proportional to $\langle \hat{\sigma}_+\hat{\sigma}_+\hat{\sigma}_-\hat{\sigma}_-\rangle$, vanishes since $\hat{\sigma}_-\hat{\sigma}_- = 0$. Indeed, only a delayed emission of the second photon is possible, so that $G^{(2)}(\mathbf{r},t;\mathbf{r},t) < G^{(2)}(\mathbf{r},t;\mathbf{r},t+\tau)$ for $\tau > 0$.

The same result holds when the quantum interaction with the free-space electromagnetic field is taken into account, having care to redefine the atomic transition frequency to include the Lamb-shift. In the case in which the electromagnetic field interacting with the atom is significantly affected by a photonic structure as an optical cavity, Eq. (3) can still be safely used if the light-matter system is in the so-called weak coupling regime. In this regime, where the atom-field coupling rate is smaller than the decay rates of both the field mode and the atomic excitation, the presence of the cavity only induces a modification of the spontaneous emission rate and of the scattered field $\mathbf{\Psi}(\mathbf{r})$. In the opposite case, when the interaction between the atomic dipole and the electromagnetic field enters the strong coupling regime, the coupling changes the energy eigenstates and Eq. (2) does not apply

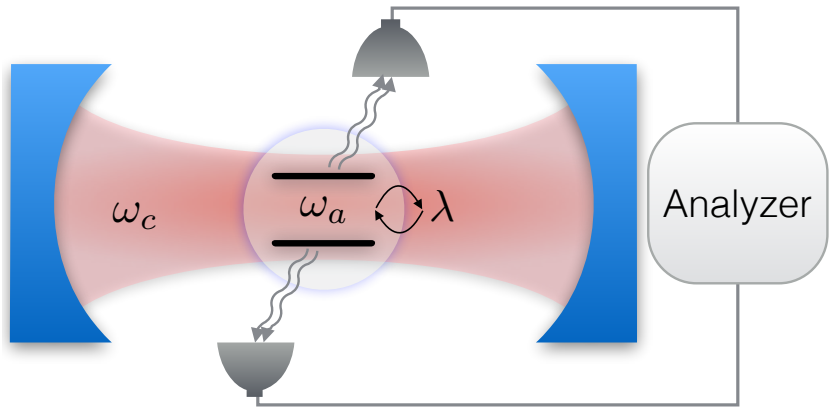

Figure 1: Sketch of the system. A two-level atom is coupled to a resonator mode. Light emitted by the atom into the external modes is detected by two photodetectors and analyzed to measure two-photon coincidence counting rates.

anymore. Nevertheless, since the shifts in the atomic frequency are of the same order of λ, in the strong coupling regime, when $\lambda/\omega_{\rm a} \ll 1$, they are small enough so that Eq. (3) is still a good approximation. We observe that the emission of bunched light by a quantum emitter dressed by an electric field has already been reported, for instance in the Jaynes Cummings model[60,61] and in resonance fluorescence,[61–63] using frequency filters. However, owing to the time-frequency uncertainty principle, the frequency-filtered correlation function, describing bunched light, can be expressed in terms of time-delayed correlation functions $G^{(2)}(\mathbf{r},t;\mathbf{r},t+\tau)$, and bunched light is observed despite $G^{(2)}(\mathbf{r},t;\mathbf{r},t)=0$.

The situation changes in the USC regime, when λ amounts to a non-negligible fraction of ω_a and the time evolution of $\hat{\sigma}_-$ can differ significantly from Eq. (2). In this case, Eq. (3) has to be replaced by[24]

$$\hat{\mathbf{E}}^{+}(\mathbf{r},t) = \hat{\mathbf{E}}^{+}_{\rm in}(\mathbf{r},t) + \mathbf{\Psi}(\mathbf{r})\,\ddot{\hat{\sigma}}^{+}_{x}(\tilde{t})\,, \tag{4}$$

where $\hat{\sigma}^{+}_{x}$ describes the positive-frequency component of $\hat{\sigma}_x$ with $\lim_{\lambda\to 0}\hat{\sigma}^{+}_{x}=\hat{\sigma}_-$. It can be obtained by expanding $\hat{\sigma}_x$ in terms of the energy eigenstates of the coupled atom-field system. If $|i\rangle$ are the eigenstates with eigenvalues $\omega_i > \omega_j$ for $i>j$, we obtain: $\hat{\sigma}^{+}_{x} = \sum_{i<j}\sigma_{ij}\,\hat{P}_{ij}$, where $\sigma_{ij}\equiv\langle i|\hat{\sigma}_x|j\rangle$ and $\hat{P}_{ij}\equiv|i\rangle\langle j|$. The second-order time derivative $\ddot{\hat{\sigma}}^{+}_{x}$ can be directly obtained by using $\hat{P}_{ij}(t)=\hat{P}_{ij}\,e^{-i\omega_{ji}t}$, where $\omega_{ji}=\omega_j-\omega_i$. It results $\ddot{\hat{\sigma}}^{+}_{x} = -\sum_{i<j}\omega^2_{ji}\,\sigma_{ij}\,\hat{P}_{ij}$.

In this case $G^{(2)}(\mathbf{r},t;\mathbf{r},t) \propto \langle \ddot{\hat{\sigma}}_x^- \ddot{\hat{\sigma}}_x^- \ddot{\hat{\sigma}}_x^+ \ddot{\hat{\sigma}}_x^+ \rangle$ and, except when $\lambda \to 0$, there is no general rule implying $G^{(2)}(\mathbf{r},t;\mathbf{r},t) = 0$.

2 Results

In order to understand how the USC regime affects the statistics of photons emitted by a single quantum emitter, we consider a generalized quantum Rabi model [29] described by the Hamiltonian ($\hbar = 1$):

$$\hat{H} = \frac{\omega_a}{2}\hat{\sigma}_z + \omega_c \hat{a}^\dagger \hat{a} + \lambda(\hat{a} + \hat{a}^\dagger)\,\hat{\mathcal{I}}_\theta\,, \tag{5}$$

where $\hat{a}^\dagger$ and $\hat{a}$ are the creation and annihilation photon operators for a single-mode cavity, ω_c is the resonance frequency of the cavity mode, $\hat{\mathcal{I}}_\theta = \cos\theta\hat{\sigma}_x + \sin\theta\hat{\sigma}_z$, and $\hat{\boldsymbol{\sigma}}$ are Pauli operators. This Hamiltonian includes a longitudinal coupling term ($\propto \hat{\sigma}_z$) which arises from the broken inversion symmetry of the atomic potential energy, and will allow us to treat not only the case of natural atoms, but also artificial atoms realised with superconducting circuits.[64] Note that in general the total Hamiltonian will also include a diamagnetic interaction term $\hat{H}_{\rm d} = \hat{H}_{\rm R} + D(\hat{a}+\hat{a}^\dagger)^2$ [65,66] which is quadratic in the cavity-field operator. While in superconducting systems such a term can be engineered and eventually made negligible, in natural atoms there is a lower bound for the coefficient of the diamagnetic term $D \geq \lambda^2/\omega_a$, with the equality valid for transitions which saturate the TRK sum rule. [67]

For a flux qubit artificial atom, the flux dependence is encoded in the angle θ: $\sin\theta = \varepsilon/\omega_a$, where ε is the flux bias and $\omega_a = \sqrt{\Delta^2 + \varepsilon^2}$, with Δ describing the qubit energy gap in the absence of the flux bias. When the flux bias is zero, $\theta = 0$ and Eq. (5) reduces to the standard quantum Rabi Hamiltonian $\hat{H}_{\rm R}$.

In circuit QED experiments, the artificial atoms can be excited by coupling them to a transmission line. Moreover, it is also possible to measure their state by detecting the reflected or emitted electromagnetic field. For example, if a semi-infinite transmission line is terminated with an inductive coupling to an artificial atom, the output voltage $\hat{V}_{\rm out}$ can

be related to the input voltage $\hat{V}_{\rm in}$ by the following relationship [68]

$$\hat{V}_{\rm out}(x,t) = -\hat{V}_{\rm in}(x,t) - m\,\dot{\hat{I}}_a(\tilde{t})\,, \tag{6}$$

where m describes the mutual inductance, $\hat{I}_a$ is the atom current operator and $\tilde{t} = t - x/v$, where v is the speed of light in the transmission line. For a flux-qubit artificial atom the current operator can be written, in the qubit energy-eigenbasis, as $\hat{I}_a = I_a\hat{\mathcal{I}}_\theta$. When the flux bias is zero, $\theta = 0$ and the current operator results to be proportional to $\dot{\hat{\sigma}}_x$. The resulting positive frequency component of the output voltage is $\hat{V}^+_{\rm out}(x,t) = -\hat{V}^+_{\rm in}(x,t) - \beta\,\dot{\hat{\mathcal{I}}}^+_\theta(\tilde{t})$, where $\beta = mI_a$. Also in this case, if the interaction of the artificial atom with the electromagnetic field does not significantly affects its dynamics, we can approximate $\dot{\hat{\mathcal{I}}}^+_\theta(\tilde{t}) \simeq -i\omega_a\hat{\sigma}_-$ so that $G^{(2)}(x,t,x,t) \propto \langle\hat{\sigma}_+\hat{\sigma}_+\hat{\sigma}_-\hat{\sigma}_-\rangle = 0$.

Our aim is to study the statistics of the photons emitted by a generic single two-level system coupled to a photonic resonator for a wide range of light-matter coupling strengths. To this end, we first focus our attention on the quantum Rabi model ($\theta = 0$) and its generalizations to include the diamagnetic term proportional to the square of the field amplitude. We will then consider the case of artificial atoms where the light-matter longitudinal coupling is present. When the normalized coupling strength λ/ω_a is not sufficiently small, the second order normalized correlation function may depend on the specific operators describing the light emitted by the atom and can be expressed as

$$g^{(2)}_O(\tau) = \frac{\langle\hat{O}^-(t)\hat{O}^-(t+\tau)\hat{O}^+(t+\tau)\hat{O}^+(t)\rangle}{\langle\hat{O}^-(t)\hat{O}^+(t)\rangle\langle\hat{O}^-(t+\tau)\hat{O}^+(t+\tau)\rangle}\,, \tag{7}$$

where $\hat{O}^\pm$ is a positive or negative frequency component operator. In this article, we present calculations for $\hat{O} \in \left[\hat{\sigma}_x, \dot{\hat{\sigma}}_x, \ddot{\hat{\sigma}}_x, \dot{\hat{\mathcal{I}}}_\theta\right]$. In the limit $\lambda/\omega_a \to 0$, all these operators provide $g^{(2)}_O(0) = 0$ as a result.

Figure 2(a) displays the energy differences between the lowest energy levels and the ground state energy as a function of the normalized coupling strength λ/ω_a obtained by nu-

merical diagonalization of the quantum Rabi Hamiltonian $\hat{H}_{\rm R}$ (blue solid curves), describing the case of a superconducting circuit. Instead, the red dashed curves have been obtained by diagonalizing the Hamiltonian $H_{\rm d}$ which includes the diamagnetic term with $D = \lambda^2/\omega_a$, modelling a natural atom coupled to a photonic resonator.

All the results displayed in Fig. 2 have been obtained at zero detuning ($\omega_c = \omega_a$). The ground state is indicated as $|\tilde{0}\rangle$ and the excited energy states have been labeled as $|\tilde{n}_{\pm}\rangle$ on the basis of the usual notation for the eigenstates of the Jaynes-Cummings (JC) eigenstates $|n_{\pm}\rangle$. When the counter-rotating terms in the Hamiltonian go to zero, each state $|\tilde{n}_{\pm}\rangle \to |n_{\pm}\rangle$ and the two states conserve their parity for all values of λ/ω_a.

We consider the system initially prepared in the state $|\tilde{2}_{-}\rangle$. The arrows in Fig. 2(a) show the available decay channels. A crossing between the energy levels $\omega_{\tilde{2}_-}$ and $\omega_{\tilde{1}_+}$ of the quantum Rabi model can be observed at $\lambda/\omega_a = g_{\rm c} \sim 0.45$. For $\lambda/\omega_a < g_{\rm c}$, the quantum Rabi model displays two possible decay channels towards the ground state: $|\tilde{2}_{-}\rangle \to |\tilde{1}_{\pm}\rangle \to |\tilde{0}\rangle$. Other possible transitions as, e.g., $|\tilde{1}_{+}\rangle \to |\tilde{1}_{-}\rangle$ or $|\tilde{2}_{-}\rangle \to |\tilde{0}\rangle$ are forbidden owing to the parity selection rule. For $\lambda/\omega_a > g_{\rm c}$, only one decay channel is allowed. The resulting zero-delay normalized second order correlation function at $t = 0$ can be written as

$$g_O^{(2)}(0) = \frac{|O_{\tilde{0},\tilde{1}_+} O_{\tilde{1}_+,\tilde{2}_-} + O_{\tilde{0},\tilde{1}_-} O_{\tilde{1}_-,\tilde{2}_-}|^2}{(|O_{\tilde{1}_+,\tilde{2}_-}|^2 + |O_{\tilde{1}_-,\tilde{2}_-}|^2)^2}, \tag{8}$$

where $O_{n,m} \equiv \langle n|\hat{O}|m\rangle$, when the two decay channels are present, and as

$$g_O^{(2)}(0) = \frac{|O_{\tilde{0},\tilde{1}_-} O_{\tilde{1}_-,\tilde{2}_-}|^2}{|O_{\tilde{1}_-,\tilde{2}_-}|^4} \tag{9}$$

after the crossing, where there is only one decay channel.

For small coupling strengths ($\lambda/\omega_a \to 0$), where the JC eigenstates are a good approximation, it results $\sigma_{0,1_\pm}\, \sigma_{1_\pm,2_-} = \pm 1/2$, and the numerator in Eq. (8) implies $g_{\sigma_x}^{(2)}(0) \to 0$. Hence the well-know result $g_{\sigma_x}^{(2)}(0) = 0$ can be interpreted as the result of complete destructive interference of the two possible paths determining the two terms in the numerator of Eq. (8).

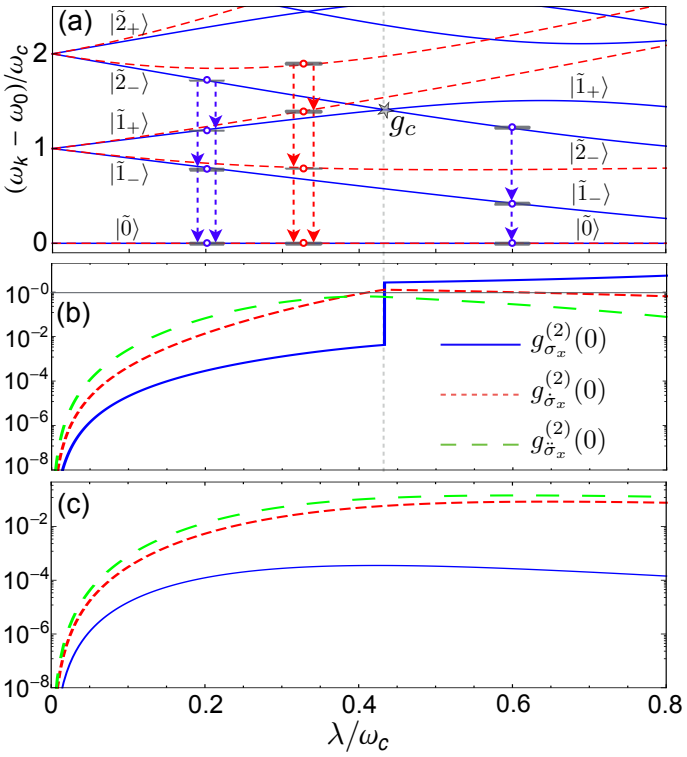

Figure 2: (a) Energy spectra of the quantum Rabi Hamiltonian $\hat{H}_{\rm R}$ (blue solid curves) and of the Hamiltonian $\hat{H}_{\rm d}$ including the diamagnetic term (red dashed curves) as a function of the normalized coupling strength λ/ω_c at zero detuning ($\omega_c = \omega_a$). The arrows describe the possible decay channels for the system prepared in the eigenstate $|\tilde{2}_-\rangle$ of $\hat{H}_{\rm R}$ (for $\lambda/\omega_c < g_c$ and $\lambda/\omega_c > g_c$) and $\hat{H}_{\rm d}$ (for $\lambda/\omega_c > g_c$) (b) Normalized second-order correlation functions $g^{(2)}_O(0)$ for $O = \sigma_x, \dot{\sigma}_x, \ddot{\sigma}_x$ as a function of λ/ω_c, for the system prepared in the initial state $|\tilde{2}_-\rangle$ of $\hat{H}_{\rm R}$ and (c) in the initial state $|\tilde{2}_-\rangle$ of $\hat{H}_{\rm d}$.

Figure 2(b) displays the three $g^{(2)}_O(0)$ with $O = \sigma_x, \dot{\sigma}_x, \ddot{\sigma}_x$ for the quantum Rabi model as a function of the normalized coupling strength λ/ω_a. We notice that, for the quantum Rabi Hamiltonian ($\theta = 0$), the operator $\dot{\hat{\sigma}}_x$ corresponds to the time derivative of the qubit current. As expected, the three curves start from zero for $\lambda/\omega_a \to 0$ and increase for increasing values of the coupling strength. We notice that $g^{(2)}_{\sigma_x}(0)$ (blue solid curve) remains below 10^{-3} for $\lambda/\omega_a < g_c$, since the corrections due to the counter-rotating terms are not able to affect the products $\sigma_{\tilde{0},\tilde{1}_\pm}\,\sigma_{\tilde{1}_\pm,\tilde{2}_-}$ so that the numerator of Eq. (8) remains very small. When $\lambda/\omega_a = g_c$, a sharp transition occurs. As shown in Fig. 2(a), for $\lambda/\omega_a > g_c$ only one decay channel is allowed and no cancellation effects are possible in the numerator of $g^{(2)}_{\sigma_x}(0)$ (see Eq.(9)) which jumps to ~ 3. The situation is different for $g^{(2)}_{\dot{\sigma}_x}(0)$ and $g^{(2)}_{\ddot{\sigma}_x}(0)$. For example, if we

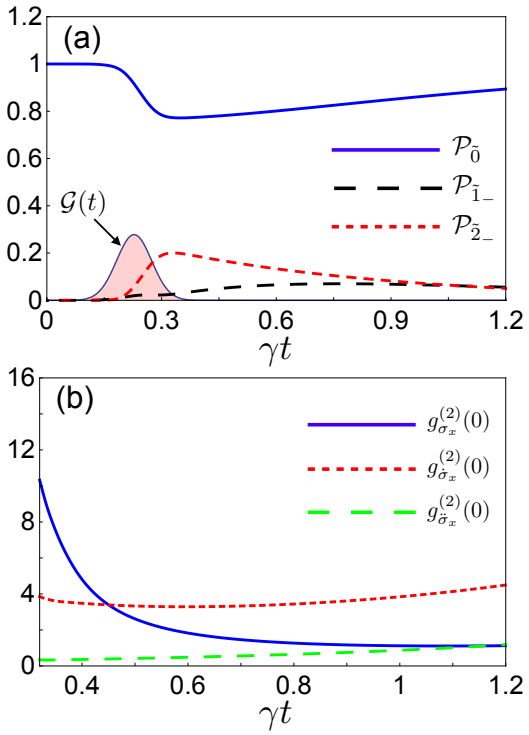

Figure 3: Two-photon excitation of the state $|\tilde{2}_-\rangle$ via a Gaussian pulse $A\,\mathcal{G}(t)\cos(\omega_d t)$, where $\mathcal{G}(t)$ is a normalized Gaussian function (shaded curve). The central frequency and the amplitude of the pulse are, respectively, $\omega_d = \omega_{\tilde{2}_-,0}/2$ and $A = 1.95$. (a) Time evolution of the populations of the three lowest energy states. (b) Zero-delay, normalized second-order correlation functions $g^{(2)}_O(0)$ for $O = \sigma_x, \dot{\sigma}_x, \ddot{\sigma}_x$ as a function of time. We used a normalized coupling strength $\lambda/\omega_c = 0.6$ and atomic and photonic loss rates $\gamma = \kappa = 10^{-3}\,\omega_c$.

consider $g^{(2)}_{\dot{\sigma}_x}(0)$ we observe that the two terms in the numerator in Eq. (8) for $\lambda/\omega_a < g_c$ have the form $\omega_{\tilde{1}_\pm,\tilde{0}}\omega_{\tilde{2}_-,\tilde{1}_\pm}\sigma_{\tilde{0},\tilde{1}_\pm}\,\sigma_{\tilde{1}_\pm,\tilde{2}_-}$. Even if $\sigma_{\tilde{0},\tilde{1}_\pm}\,\sigma_{\tilde{1}_\pm,\tilde{2}_-} \simeq \pm 1/2$, for increasing values of the coupling strength the transition frequency $\omega_{\tilde{2}_-,\tilde{1}_+}$ decreases significantly, lowering one of these two terms in the numerator so that $g^{(2)}_{\dot{\sigma}_x}(0)$ can differ significantly from zero even before $\lambda/\omega_a = g_c$. Figure 2(c) displays the three $g^{(2)}_O(0)$ for the system described by $\hat{H}_{\rm d}$ as a function of the normalized coupling strength λ/ω_a under the same conditions used to derive the results in Fig. 2(b). As shown in Fig. 2(a), in this case no level crossings occur and two decay channels are always present. The normalized correlation functions are described by Eq. (8). Owing to the destructive interference, $g^{(2)}_{\sigma_x}(0)$ remains very small (below 10^{-4}) even at larger coupling strengths. On the contrary, owing to the differences between the transition frequencies of the two available decay paths, $g^{(2)}_{\dot{\sigma}_x}(0)$ and $g^{(2)}_{\ddot{\sigma}_x}(0)$ display experimentally detectable

deviations from the standard (weak coupling) result $g_O^{(2)}(0) = 0$. The system can be experimentally prepared in the state $|\tilde{2}_-\rangle$ by exciting the qubit or the cavity with a sequence of two resonant π-pulses, determining the sequential transitions $|\tilde{0}\rangle \rightarrow |\tilde{1}_-\rangle \rightarrow |\tilde{2}_-\rangle$. The system can also be prepared by two-photon excitation: $|\tilde{0}\rangle \rightarrow |\tilde{2}_-\rangle$. In this latter case, the resulting state will be the superposition $|\psi(0)\rangle = \sqrt{1-|\alpha|^2}|\tilde{0}\rangle + \alpha|\tilde{2}_-\rangle$ with $\alpha \ll 1$. Using this as initial state, the obtained $g_O^{(2)}(0)$ can be significantly higher, reproducing the curves displayed in Fig. 2(b) and 2(c) divided, however, approximately by the factor $|\alpha|^2$. Figure 3 displays a numerical test of this excitation mechanism, obtained using $\lambda/\omega_c = 0.6$. The system Hamiltonian, including the external pulse feeding the cavity is $\hat{H}_{\rm R} + A\,\mathcal{G}(t)\cos(\omega_d t)(\hat{a}+\hat{a}^\dagger)$, where $\mathcal{G}(t)$ is a normalized Gaussian function. The central frequency and the amplitude of the pulse are, respectively, $\omega_d = \omega_{\tilde{2}_-,0}/2$ and $A = 1.95$. The influence of the cavity-field damping and atomic decay on the process are taken into account by using the master-equation approach in the dressed picture.[38,69] We consider the system interacting with zero-temperature baths. The master equation is obtained by using the Born-Markov approximation without the post-trace RWA.[70] We use for the decay rates of the qubit (γ) and the cavity (κ): $\gamma = \kappa = 10^{-3}\,\omega_c$. Figure 3(a) shows the populations of the three lowest energy states. The system is initially in its ground state $|\tilde{0}\rangle$ and, after the arrival of the Gaussian pulse (shaded curve), the state $|\tilde{2}_-\rangle$ reaches a population of about 0.2, depending on the pulse amplitude. As times goes on, also the lower energy state $|\tilde{1}_-\rangle$ populates owing to the decay $|\tilde{2}_-\rangle \rightarrow |\tilde{1}_-\rangle$. Figure 3(b) displays the time evolution of the three equal-time $g_O^{(2)}(0)$ with $O = \sigma_x, \dot{\sigma}_x, \ddot{\sigma}_x$. All of them are different from zero and, as expected, they display larger values than the corresponding ones (at $\lambda = 0.6\omega_c$) in Fig. 2(b). Figure 4 shows results in the case for which a longitudinal coupling between the qubit and the resonator field is present ($\theta \neq 0$). We use a zero-bias qubit gap $\Delta/\omega_c = 0.5$ GHz and a qubit-resonator coupling rate $\lambda/\omega_c = 0.2$. Figure 4(a) displays the energy spectrum for the lowest energy levels of $\hat{H}$ as a function of the normalized flux bias ε/ω_c. The arrows describe the possible decay channels for the system prepared in the eigenstate $|\tilde{1}_+\rangle$. For $\varepsilon = 0$, the parity selection rule implies that only the one-photon

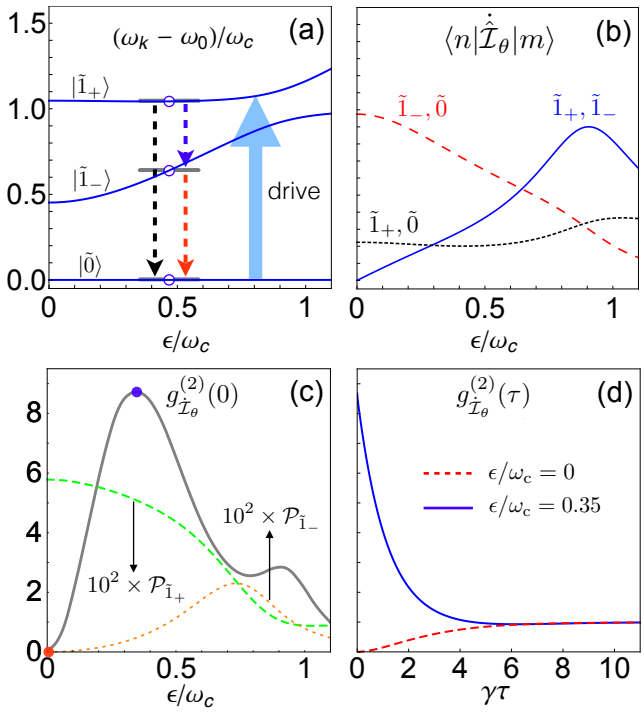

Figure 4: (a) Energy spectrum of the generalized Rabi Hamiltonian $\hat{H}$ (blue solid curves) as a function of the normalized flux offset ε/ω_c. We set the zero-bias qubit gap to $\Delta/\omega_c = 0.5$ GHz and consider a qubit-resonator coupling rate $\lambda/\omega_c = 0.2$. The dashed blue arrows describe the possible decay channels for the system prepared in the eigenstate $|\tilde{1}_+\rangle$, while the solid red arrow describes the system excitation by an applied drive. (b) Matrix elements $\langle n|\dot{\mathcal{I}}_\theta|m\rangle$ for the transitions $|\tilde{1}_\pm\rangle \rightarrow |\tilde{0}\rangle$ and $|\tilde{1}_+\rangle \rightarrow |\tilde{1}_-\rangle$ as a function of ε/ω_c. (c) Qubit normalized second-order correlation function $g^{(2)}_{\dot{\mathcal{I}}_\theta}(0)$ as a function of ε/ω_c (grey solid curve) for the system driven towards the $|\tilde{1}_+\rangle$ state by applying to the resonator a continuous-wave optical drive of amplitude $A/\gamma = 0.25$. The steady-state populations $\mathcal{P}_{\tilde{1}_-}$ (orange dotted curve) and $\mathcal{P}_{\tilde{1}_+}$ (green dashed curve) of the $|\tilde{1}_-\rangle$ and $|\tilde{1}_+\rangle$ states are also dispayed. Populations of higher energy levels are below 10^{-4} and are not reported in the figure. (d) Qubit steady-state time-delayed normalized second-order correlation function $g^{(2)}_{\dot{\mathcal{I}}_\theta}(\tau)$ obtained for $\varepsilon/\omega_c = 0$ (red dashed curve) and for $\varepsilon/\omega_c = 0.35$ (blue solid curve). The decay rates for the qubit and the resonator are $\gamma = \kappa = 5 \times 10^{-4}\,\omega_c$.

transition $|\tilde{1}_+\rangle \rightarrow |\tilde{0}\rangle$ and as a consequence $g^{(2)}_O(0) = 0$ is expected. For $\varepsilon \neq 0$, the parity selection rule is broken and all the available downward spontaneous transitions are allowed (see Fig 4(b)). In order to present results that can be experimentally studied more easily, we calculate the steady-state normalized correlation function $g^{(2)}_{\dot{\mathcal{I}}_\theta}(0)$ for the field emitted by the qubit after continuous-wave pumping of the resonator with a drive resonant with the transition $|\tilde{0}\rangle \leftrightarrow |\tilde{1}_+\rangle$. The system Hamiltonian including the drive is $\hat{H} + A\cos(\omega_d t)(\hat{a} + \hat{a}^\dagger)$

with $\omega_d = \omega_{\tilde{1}_+,0}$. Also in this case, the influence of the cavity-field damping and atomic decay on the process are taken into account by using the master-equation approach in the dressed picture.[38,69] We consider the system interacting with zero-temperature baths. The master equation is obtained by using the Born-Markov approximation without the post-trace RWA.[70] We use for the decay rates of the qubit (γ) and the cavity (κ): $\gamma = \kappa = 5 \times 10^{-4}\,\omega_c$. Moreover, we use an excitation amplitude $A/\gamma = 0.25$ able to provide a steady-state population for the state $|\tilde{1}_+\rangle$ ranging between 1% and 6% depending on the value of ε [see Fig. 4(c)]. According to Eq. (6), the measured second-order correlation function can be obtained from Eq. (7) by using $\hat{O} = \dot{\hat{\mathcal{I}}}_\theta$. Figure 4(c) shows the steady-state, zero-delay qubit normalized correlation function as a function of the flux bias. Also in this case, we find that it is significantly different from zero, reaching its maximum (~ 8.7) at $\varepsilon/\omega_c \sim 0.35$. The shape of the curve in Fig. 4(c) and the position of its maximum mainly depend on the dependence on ε of the matrix elements showed in Fig 4(b). Figure 4(d) displays the qubit steady-state time-delayed normalized second-order correlation function $g^{(2)}_{\dot{\mathcal{I}}_\theta}(\tau)$ obtained for $\varepsilon/\omega_c = 0$ (red-dashed curve) and for $\varepsilon/\omega_c = 0.35$ (where $g^{(2)}_{\dot{\mathcal{I}}_\theta}(0)$ is maximum) (blue continuous curve). For $\varepsilon/\omega_c = 0$, the expected antibunching effect: $g^{(2)}_{\dot{\mathcal{I}}_\theta}(\tau) > g^{(2)}_{\dot{\mathcal{I}}_\theta}(0)$ can be observed. On the contrary, the blue continuous curve shows a photon bunching effect: $g^{(2)}_{\dot{\mathcal{I}}_\theta}(\tau) < g^{(2)}_{\dot{\mathcal{I}}_\theta}(0)$. As expected, both the two curves tend to 1 for $\tau \to \infty$, indicating the loss of correlation between the emitted photons.

3 Conclusions

The first observation of antibunching in the light emitted by a two level atom, which dates back to forty years ago by Kimble, Dagenais, and Mandel,[2] has been interpreted by many as a definitive proof of the quantization of the electromagnetic field, and it still stands as one of the iconic results of quantum optics. In this paper, we show for the first time that this is not a universal feature, and that a single two-level system, physically instantiated in a real or an artificial atom, can emit bunched light, exhibiting a zero-delay two-photon correlation function different from zero. The effect here described provides clear evidence of how an atom can lose its identity when ultrastrongly interacting with a photonic resonator.

The possibility to engineer the quantum properties of light emitted by single emitters has revealed itself an useful tool to generate the non-classical states of light[71] required by quantum metrology applications.[72] Apart from their fundamental importance our results, demonstrating the possibility to tune photon correlations in situ by an external control parameter, could thus also find practical applications in the ongoing quest toward the realization of practical quantum devices.

Acknowledgements

L. G. and S.D.L. acknowledge support from EPSRC Grant No. EP/M003183/1. S.D.L. has support from the Royal Society Research Fellowship program.

References

(1) Carmichael, H. J.; Walls, D. F. Proposal for the measurement of the resonant Stark effect by photon correlation techniques. *J. Phys. B: At. Mol. Phys.* **1976**, *9*, L43.

(2) Kimble, H. J.; Dagenais, M.; Mandel, L. Photon antibunching in resonance fluorescence. *Phys. Rev. Lett.* **1977**, *39*, 691.

(3) Basché, T.; Moerner, W. E.; Orrit, M.; Talon, H. Photon antibunching in the fluorescence of a single dye molecule trapped in a solid. *Phys. Rev. Lett.* **1992**, *69*, 1516.

(4) Michler, P.; Imamoğlu, A.; Mason, M. D.; Carson, P. J.; Strouse, G. F.; Buratto, S. K. Quantum correlation among photons from a single quantum dot at room temperature. *Nature* **2000**, *406*, 968–970.

(5) Press, D.; Götzinger, S.; Reitzenstein, S.; Hofmann, C.; Löffler, A.; Kamp, M.; Forchel, A.; Yamamoto, Y. Photon antibunching from a single quantum-dot-microcavity system in the strong coupling regime. *Phys. Rev. Lett.* **2007**, *98*, 117402.

(6) Yuan, Z.; Kardynal, B. E.; Stevenson, R. M.; Shields, A. J.; Lobo, C. J.; Cooper, K.; Beattie, N. S.; Ritchie, D. A.; Pepper, M. Electrically driven single-photon source. *Science* **2002**, *295*, 102–105.

(7) Brouri, R.; Beveratos, A.; Poizat, J.-P.; Grangier, P. Photon antibunching in the fluorescence of individual color centers in diamond. *Opt. Lett.* **2000**, *25*, 1294–1296.

(8) Kurtsiefer, C.; Mayer, S.; Zarda, P.; Weinfurter, H. Stable solid-state source of single photons. *Physical review letters* **2000**, *85*, 290.

(9) Högele, A.; Galland, C.; Winger, M.; Imamoğlu, A. Photon antibunching in the photoluminescence spectra of a single carbon nanotube. *Phys. Rev. Lett.* **2008**, *100*, 217401.

(10) Houck, A. A.; Schuster, D. I.; Gambetta, J. M.; Schreier, J. A.; Johnson, B. R.; Chow, J. M.; Frunzio, L.; Majer, J.; Devoret, M. H.; Girvin, S. M.; Schoelkopf, R. J. Generating single microwave photons in a circuit. *Nature* **2007**, *449*, 328–331.

(11) Michler, P.; Kiraz, A.; Becher, C.; Schoenfeld, W. V.; Petroff, P. M.; Zhang, L.; Hu, E.; Imamoglu, A. A quantum dot single-photon turnstile device. *Science* **2000**, *290*, 2282–2285.

(12) Bennett, C. H.; Brassard, G.; Mermin, N. D. Quantum cryptography without Bell's theorem. *Phys. Rev. Lett.* **1992**, *68*, 557.

(13) Bouwmeester, D.; Ekert, A.; Zeilinger, A. *The physics of quantum information*; Springer, Berlin, 2000; Vol. 3.

(14) Knill, E.; Laflamme, R.; Milburn, G. J. A scheme for efficient quantum computation with linear optics. *Nature* **2001**, *409*, 46–52.

(15) Pelton, M.; Santori, C.; Vučković, J.; Zhang, B.; Solomon, G. S.; Plant, J.; Yamamoto, Y. Efficient source of single photons: a single quantum dot in a micropost microcavity. *Phys. Rev. Lett.* **2002**, *89*, 233602.

(16) Chang, W.-H.; Chen, W.-Y.; Chang, H.-S.; Hsieh, T.-P.; Chyi, J.-I.; Hsu, T.-M. Efficient single-photon sources based on low-density quantum dots in photonic-crystal nanocavities. *Phys. Rev. Lett.* **2006**, *96*, 117401.

(17) De Liberato, S.; Ciuti, C.; Carusotto, I. Quantum vacuum radiation spectra from a semiconductor microcavity with a time-modulated vacuum Rabi frequency. *Phys. Rev. Lett.* **2007**, *98*, 103602.

(18) De Liberato, S.; Gerace, D.; Carusotto, I.; Ciuti, C. Extracavity quantum vacuum radiation from a single qubit. *Phys. Rev. A* **2009**, *80*, 053810.

(19) Ashhab, S.; Nori, F. Qubit-oscillator systems in the ultrastrong-coupling regime and their potential for preparing nonclassical states. *Phys. Rev. A* **2010**, *81*, 042311.

(20) Ai, Q.; Li, Y.; Zheng, H.; Sun, C. P. Quantum anti-Zeno effect without rotating wave approximation. *Phys. Rev. A* **2010**, *81*, 042116.

(21) Cao, X.; You, J.; Zheng, H.; Kofman, A.; Nori, F. Dynamics and quantum Zeno effect for a qubit in either a low-or high-frequency bath beyond the rotating-wave approximation. *Phys. Rev. A* **2010**, *82*, 022119.

(22) Cao, X.; You, J.; Zheng, H.; Nori, F. A qubit strongly coupled to a resonant cavity: asymmetry of the spontaneous emission spectrum beyond the rotating wave approximation. *New J. Phys.* **2011**, *13*, 073002.

(23) Stassi, R.; Ridolfo, A.; Di Stefano, O.; Hartmann, M.; Savasta, S. Spontaneous Conversion from Virtual to Real Photons in the Ultrastrong-Coupling Regime. *Phys. Rev. Lett.* **2013**, *110*, 243601.

(24) Garziano, L.; Ridolfo, A.; Stassi, R.; Di Stefano, O.; Savasta, S. Switching on and off of ultrastrong light-matter interaction: Photon statistics of quantum vacuum radiation. *Phys. Rev. A* **2013**, *88*, 063829.

(25) Huang, J.-F.; Law, C. Photon emission via vacuum-dressed intermediate states under ultrastrong coupling. *Phys. Rev. A* **2014**, *89*, 033827.

(26) Cacciola, A.; Di Stefano, O.; Stassi, R.; Saija, R.; Savasta, S. Ultrastrong Coupling of Plasmons and Excitons in a Nanoshell. *ACS Nano* **2014**, *8*, 11483–11492.

(27) Garziano, L.; Stassi, R.; Ridolfo, A.; Di Stefano, O.; Savasta, S. Vacuum-induced symmetry breaking in a superconducting quantum circuit. *Phys. Rev. A* **2014**, *90*, 043817.

(28) De Liberato, S. Light-Matter Decoupling in the Deep Strong Coupling Regime: The Breakdown of the Purcell Effect. *Phys. Rev. Lett.* **2014**, *112*, 016401.

(29) Garziano, L.; Stassi, R.; Macrì, V.; Kockum, A.; Savasta, S.; Nori, F. Multiphoton quantum Rabi oscillations in ultrastrong cavity QED. *Phys. Rev. A* **2015**, *92*, 063830.

(30) Zhao, Y.-J.; Liu, Y.-L.; Liu, Y.-X.; Nori, F. Generating nonclassical photon states via longitudinal couplings between superconducting qubits and microwave fields. *Phys. Rev. A* **2015**, *91*, 053820.

(31) Baust, A. et al. Ultrastrong coupling in two-resonator circuit QED. *Phys. Rev. B* **2016**, *93*, 214501.

(32) Wang, Y.; Zhang, J.; Wu, C.; You, J. Q.; Romero, G. Holonomic quantum computation in the ultrastrong-coupling regime of circuit QED. *Phys. Rev. A* **2016**, *94*, 012328.

(33) Stassi, R.; Savasta, S.; Garziano, L.; Spagnolo, B.; Nori, F. Output field-quadrature measurements and squeezing in ultrastrong cavity-QED. *New J. Phys.* **2016**, *18*.

(34) Garziano, L.; Macrí, V.; Stassi, R.; Di Stefano, O.; Nori, F.; Savasta, S. One photon can simultaneously excite two or more atoms. *Phys. Rev. Lett.* **2016**, *117*, 043601.

(35) Jaako, T.; Xiang, Z.-L.; Garcia-Ripoll, J. J.; Rabl, P. Ultrastrong-coupling phenomena beyond the Dicke model. *Phys. Rev. A* **2016**, *94*, 033850.

(36) Shen, L.-T.; Yang, Z.-B.; Wu, H.-Z.; Zheng, S.-B. Ground state of an ultrastrongly coupled qubit-oscillator system with broken inversion symmetry. *Phys. Rev. A* **2016**, *93*, 063837.

(37) Kockum, A. F.; Miranowicz, A.; Macrí, V.; Savasta, S.; Nori, F. Deterministic quantum nonlinear optics with single atoms and virtual photons. *arXiv:1701.05038* **2017**,

(38) Ridolfo, A.; Leib, M.; Savasta, S.; Hartmann, M. J. Photon Blockade in the Ultrastrong Coupling Regime. *Phys. Rev. Lett.* **2012**, *109*, 193602.

(39) Ridolfo, A.; Savasta, S.; Hartmann, M. J. Nonclassical Radiation from Thermal Cavities in the Ultrastrong Coupling Regime. *Phys. Rev. Lett.* **2013**, *110*, 163601.

(40) Le Boité, A.; Hwang, M.-J.; Nha, H.; Plenio, M. B. Fate of photon blockade in the deep strong-coupling regime. *Phys. Rev. A* **2016**, *94*, 033827.

(41) Günter, G.; Anappara, A. A.; Hees, J.; Sell, A.; Biasiol, G.; Sorba, L.; De Liberato, S.; Ciuti, C.; Tredicucci, A.; Leitenstorfer, A.; Huber, R. Sub-cycle switch-on of ultrastrong light–matter interaction. *Nature* **2009**, *458*, 178–181.

(42) Forn-Díaz, P.; Lisenfeld, J.; Marcos, D.; García-Ripoll, J.; Solano, E.; Harmans, C.; Mooij, J. Observation of the Bloch-Siegert shift in a qubit-oscillator system in the ultrastrong coupling regime. *Phys. Rev. Lett.* **2010**, *105*, 237001.

(43) Niemczyk, T.; Deppe, F.; Huebl, H.; Menzel, E.; Hocke, F.; Schwarz, M.; García-Ripoll, J.; Zueco, D.; Hümmer, T.; Solano, E.; Marx, A.; Gross, R. Circuit quantum electrodynamics in the ultrastrong-coupling regime. *Nature Phys.* **2010**, *6*, 772–776.

(44) Schwartz, T.; Hutchison, J.; Genet, C.; Ebbesen, T. Reversible switching of ultrastrong light-molecule coupling. *Phys. Rev. Lett.* **2011**, *106*, 196405.

(45) Geiser, M.; Castellano, F.; Scalari, G.; Beck, M.; Nevou, L.; Faist, J. Ultrastrong Coupling Regime and Plasmon Polaritons in Parabolic Semiconductor Quantum Wells. *Phys. Rev. Lett.* **2012**, *108*, 106402.

(46) Scalari, G.; Maissen, C.; Turčinková, D.; Hagenmüller, D.; De Liberato, S.; Ciuti, C.; Reichl, C.; Schuh, D.; Wegscheider, W.; Beck, M.; Faist, J. Ultrastrong Coupling of the Cyclotron Transition of a 2D Electron Gas to a THz Metamaterial. *Science* **2012**, *335*, 1323–1326.

(47) Gambino, S.; Mazzeo, M.; Genco, A.; Di Stefano, O.; Savasta, S.; Patane, S.; Ballarini, D.; Mangione, F.; Lerario, G.; Sanvitto, D.; Gigli, G. Exploring Light–Matter

Interaction Phenomena under Ultrastrong Coupling Regime. *ACS Photonics* **2014**, *1*, 1042–1048.

(48) Goryachev, M.; Farr, W.; Creedon, D.; Fan, Y.; Kostylev, M.; Tobar, M. High-cooperativity cavity QED with magnons at microwave frequencies. *Phys. Rev. Applied* **2014**, *2*, 054002.

(49) Maissen, C.; Scalari, G.; Valmorra, F.; Beck, M.; Faist, J.; Cibella, S.; Leoni, R.; Reichl, C.; Charpentier, C.; Wegscheider, W. Ultrastrong coupling in the near field of complementary split-ring resonators. *Physical Review B* **2014**, *90*, 205309.

(50) Yoshihara, F.; Fuse, T.; Ashhab, S.; Kakuyanagi, K.; Saito, S.; Semba, K. Superconducting qubit-oscillator circuit beyond the ultrastrong-coupling regime. *Nat. Phys.* **2017**, *13*, 44–47.

(51) Chen, Z.; Wang, Y.; Li, T.; Tian, L.; Qiu, Y.; Inomata, K.; Yoshihara, F.; Han, S.; Nori, F.; Tsai, J.; You, J. Multi-photon sideband transitions in an ultrastrongly-coupled circuit quantum electrodynamics system. *arXiv preprint arXiv:1602.01584* **2016**,

(52) Forn-Díaz, P.; García-Ripoll, J.; Peropadre, B.; Orgiazzi, J.-L.; Yurtalan, M.; Belyansky, R.; Wilson, C.; Lupascu, A. Ultrastrong coupling of a single artificial atom to an electromagnetic continuum in the nonperturbative regime. *Nature Phys.* **2017**, *13*, 39–43.

(53) Bozyigit, D.; Lang, C.; Steffen, L.; Fink, J. M.; Eichler, C.; Baur, M.; Bianchetti, R.; Leek, P. J.; Filipp, S.; da Silva, M. P.; Blais, A.; Wallraff, A. Antibunching of microwave-frequency photons observed in correlation measurements using linear detectors. *Nat. Phys.* **2011**, *7*, 154–158.

(54) Lang, C.; Bozyigit, D.; Eichler, C.; Steffen, L.; Fink, J. M.; Abdumalikov, A. A.; Baur, M.; Filipp, S.; da Silva, M. P.; Blais, A.; Wallraff, A. Observation of Resonant

Photon Blockade at Microwave Frequencies Using Correlation Function Measurements. *Phys. Rev. Lett.* **2011**, *106*, 243601.

(55) Fink, J. M.; Dombi, A.; Vukics, A.; Wallraff, A.; Domokos, P. Observation of the Photon-Blockade Breakdown Phase Transition. *Phys. Rev. X* **2017**, *7*, 011012.

(56) Carusotto, I.; Ciuti, C. Quantum fluids of light. *Rev. Mod. Phys.* **2013**, *85*, 299–366.

(57) Milonni, P. *The Quantum Vacuum: An Introduction to Quantum Electrodynamics*; Academic Press, 1994.

(58) Milonni, P.; James, D. F. V.; Fearn, H. Photodetection and causality in quantum optics. *Phys. Rev. A* **1995**, *52*, 1525.

(59) Glauber, R. J. The quantum theory of optical coherence. *Phys. Rev.* **1963**, *130*, 2529.

(60) del Valle, E.; Gonzalez-Tudela, A.; Laussy, F. P.; Tejedor, C.; Hartmann, M. J. Theory of Frequency-Filtered and Time-Resolved N-Photon Correlations. *Phys. Rev. Lett.* **2012**, *109*, 183601.

(61) A. Gonzalez-Tudela, C. T. M. J. H., F. P. Laussy; del Valle, E. Two-photon spectra of quantum emitters. *New J. Phys.* **2013**, *15*.

(62) Peiris, M.; Petrak, B.; Konthasinghe, K.; Yu, Y.; Niu, Z. C.; Muller, A. Two-color photon correlations of the light scattered by a quantum dot. *Phys. Rev. B* **2015**, *91*, 195125.

(63) Peiris, M.; Konthasinghe, K.; Muller, A. Franson Interference Generated by a Two-Level System. *Phys. Rev. Lett.* **2017**, *118*, 030501.

(64) You, J.; Nori, F. Atomic physics and quantum optics using superconducting circuits. *Nature* **2011**, *474*, 589–597.

(65) Tufarelli, T.; McEnery, K.; Maier, S.; Kim, M. Signatures of the A^2 term in ultrastrongly coupled oscillators. *Phys. Rev. A* **2015**, *91*, 063840.

(66) García-Ripoll, J.; Peropadre, B.; De Liberato, S. Light-matter decoupling and A^2 term detection in superconducting circuits. *Sci. Rep.* **2015**, *5*, 125433.

(67) Nataf, P.; Ciuti, C. No-go theorem for superradiant quantum phase transitions in cavity QED and counter-example in circuit QED. *Nat. Comm.* **2010**, *1*, 72.

(68) Girvin, S. Circuit QED: Superconducting Qubits Coupled to Microwave Photons, Proceedings of the Les Houches Summer School. *(Oxford University Press, New York, NY)* **2014**, *Vol. 96*.

(69) Beaudoin, F.; Gambetta, J.; Blais, A. Dissipation and ultrastrong coupling in circuit QED. *Phys. Rev. A* **2011**, *84*, 043832.

(70) Ma, K. K.; Law, C. Three-photon resonance and adiabatic passage in the large-detuning Rabi model. *Phys. Rev. A* **2015**, *92*, 023842.

(71) Sánchez Muñoz, C.; del Valle, E.; González Tudela, A.; Müller, K.; Lichtmannecker, S.; Kaniber, M.; Tejedor, C.; J., F. J.; P., L. F. Emitters of N-photon bundles. *Nature Photonics* **2014**, *8*, 550–555.

(72) Giovannetti, V.; Lloyd, S.; Maccone, L. Quantum-enhanced measurements: beating the standard quantum limit. *Science* **2004**, *306*, 1330–1336.

Graphical TOC Entry